KERNFORSCHUNGSZENTRUM

KARLSRUHE

Backscattering of 1 MeV He$^+$ on SiC

M.-A. Nicolet, H. R. Bilger, O. Meyer
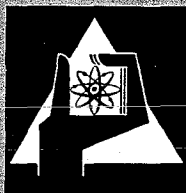
Institut für Angewandte Kernphysik, Kernforschungszentrum Karlsruhe

Backscattering of 1 MeV He+ on SiC

By

M.-A. Nicolet[1]), H. R. Bilger[2]), and O. Meyer

Backscattering measurements of 1 MeV ^{4}He+ ions on SiC were performed and compared to similar measurements on a diamond-type lattice (Si). The planar channels of SiC measured at angles 0 to 2π and 7° off the c-axis display the same dip pattern as in Si, whereas the axial channels along the $(1\bar{1}0)$ planes in Si show distinct differences to those in the equivalent $(2\bar{1}\bar{1}0)$ planes in SiC. This behaviour is explained with the model of hexagonal polytype 6H. A case of SiC with a mixed diamond–hexagonal-type backscattering pattern is also presented. Comparison to X-ray data of the same crystals is given. This study establishes the usefulness of backscattering in structure identification such as polytypism in SiC.

Rückstreuungsmessungen von 1 MeV ^{4}He+-Ionen an SiC und an Si wurden durchgeführt, die Ergebnisse verglichen. Die orientierungsabhängige Ausbeute, hervorgerufen durch den Channeling-Effekt in den Kristallebenen von SiC bei einer 360°-Rotation um die c-Achse, die unter 7° zur Ioneneinfallsrichtung geneigt war, zeigte dieselbe Struktur wie für Si. Dagegen ergaben Messungen an den Kristallachsen längs der $(1\bar{1}0)$-Ebenen in Si ausgeprägte Unterschiede im Vergleich mit den Achsen längs der entsprechenden $(2\bar{1}\bar{1}0)$-Ebenen in SiC. Eine Erklärung mit dem Modell des hexagonalen Polytyps 6 H wird gegeben. Auch der Fall eines SiC-Polykristalls, bestehend aus einer Mischung von Diamant- und hexagonaler Struktur, wurde untersucht, Vergleiche mit Röntgenanalysen an denselben Kristallen wurden durchgeführt. Die Untersuchung zeigt, daß die Rückstreuung von Ionen eine geeignete Methode ist, um Polytypen, wie z. B. SiC, zu identifizieren.

1. Introduction

The investigation of single crystals with backscattering [1] of He+ ions in the MeV range provides valuable additional data about the crystal structure with a depth resolution down to about 100 Å, at depths up to a few microns below the surface. X-ray analyses usually give integral information about the crystal. As an example, the 8 keV K_α line of Cu used for X-ray analysis has a mean range of 70 μm in SiC [2], while the mean range of 1 MeV He+ ions in the same material is 3.8 μm [3]. The energy analysis of backscattered ions furthermore allows one to identify the mass of the target atom, which is important in ion implantation studies [4], and to select a certain depth in the crystal for analysis simply by evaluating corresponding portions of the energy spectrum. In this way it is possible to obtain information about the structure down to thicknesses of a few unit cells [5] (see also Appendix A).

Besides delivering additional crystallographic data [6][3]), backscattering may become an interesting tool in the study of SiC as a material for high-temperature electronic devices [7].

---

[1]) On leave from California Institute of Technology, Pasadena, California 91109.

[2]) On leave from Oklahoma State University, Stillwater, Oklahoma 74074.

[3]) In this reference, evaluation of photographed blocking patterns is used to study crystal structures.

2. Axial and Planar Channeling

Lindhard's theory as given in reference [8] is used throughout this paper. The fraction of backscattered particles in the minimum of a dip, χ, depends on the surface density of target atoms, which in turn is given by the average spacing d_a of atoms along rows in axial channeling, or by the average spacing d_p of the planes in planar channeling. The critical angles ψ depend further on the charge density in the strings or planes, respectively.

For axial channeling, we use the estimates [8]:

$$\chi_a = \text{(backscattering events in the dip minimum)/(random events)}$$

$$= \pi\, r^2\, N\, d_a \tag{1}$$

(r is approximated by the Thomas-Fermi radius a, N is the volume density of target atoms),

$$\psi_{1/1\,a} = \text{full width at half dip depth} = \left(\frac{2\,Z_1\,\overline{Z}_2\,q^2}{\pi\,\varepsilon_0\,d_a\,E}\right)^{1/2} \text{(MKS units)}$$

or

$$\psi_{1/1\,a}\ (\text{deg}) \doteq 0.615\left(\frac{Z_1\,\overline{Z}_2}{d_a\,(\text{Å})\,E\,(\text{MeV})}\right)^{1/2} \tag{2}$$

(Z_1, $\overline{Z}_2$ charge numbers of projectile and target atoms, respectively, E energy of projectile).

For planar channels, we use [8]:

$$\chi_p = \frac{2\,a}{d_p}, \tag{3}$$

$$\psi_{1/1\,p} = \left(\frac{Z_1\,Z_2\,q^2\,N\,d_p\,a}{\pi\,\varepsilon_0\,E}\right)^{1/2}. \tag{4}$$

Studies [8] have since shown that equations (2) and (4) are correct within 25%, and equations (1) and (3) within a factor of about 2. The extension to nonequal spacing of planes or atoms in a string is straightforward and has been confirmed.

Thus, the parameters d_a and d_p determine the depths of the dips in channeling measurements. This fact has been used to identify the channels in addition to their position. More details are given in Appendix B.

3. SiC Polytype 6H

The polytypes of SiC are classified according to their lattice structures in cubic (C), hexagonal (H), and rhombohedral (R) modifications [5]. Of those, 6H is the most frequent polytype. It is thus discussed in some detail in this paper.

Fig. 1 is a sideview of the model of SiC 6H. The c-axis of its hexagonal unit cell spans six layers of close-packed planes of SiC with a stacking sequence ... ABCACB .... In Fig. 1, the terminations of the model on the left and right are chosen to emphasize this fact. The unit cell can thus be subdivided into two sublayers in the c-direction, where each sublayer is close-packed and of the zincblende structure. The cubic cell of the lower sublayer is partly shown in Fig. 1. Referred to the lower sublayer, the upper sublayer has a twist

Fig. 1. Model of the structure of SiC polytype 6H. The unit cell is hexagonal with dimensions $a = b = 3.078$ Å and $c = 6 \times 2.518$ Å $= 15.11$ Å [5]. Also shown is part of the cubic cell of the lower sublayer to visualize the cubic structure of the sublayer. The edge of the cubic cell is $\sqrt{2}\,a = 4.353$ Å
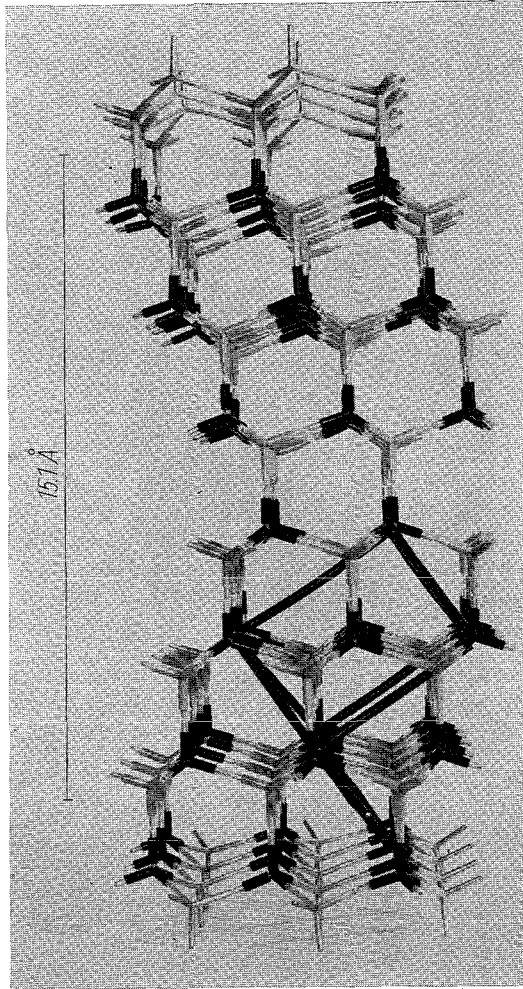
of 60° around the c-axis (which is identical to the $[111]_c$ axis of the cubic cell).[4]) The polytype 6H is thus an intimate layered mixture with a ratio of 1:1 of two cubic SiC (or β-SiC) crystals rotated against each other by 60° around their common $[111]_c$ direction. The length of the c-axis is twice the body diagonal of the cubic cell. In the following, planes and directions have been expressed both in the cubic cell and the hexagonal unit cell as reference systems. Table 1 gives indices of some directions and planes in both coordinate systems. Their relative position is chosen such that the x-axis of the cubic system, projected onto the $(a\,b)$ plane of the hexagonal system, lies between a and b.

4. Channeling and Backscattering in SiC 6H — Theoretical Considerations

This structure differs from the diamond structure in two interesting ways. First, it has a sixfold symmetry in the c-axis, while that of the diamond lattice in the $\langle 111 \rangle_c$ directions is threefold. Second, the diamond lattice exhibits large voids when viewed in a $\langle 110 \rangle_c$ direction, while these channels are interrupted in SiC 6H by every other sublayer because of their different relative orientation. This is shown in Fig. 2, where the model of Fig. 1 is shown in an oblique view, looking down a $\langle 110 \rangle_c$ channel of the upper sublayer. As the picture shows, the lower introduces 2 Si and 2 C into the channel, along one line. The exact positions of these atoms relative to the $\langle 110 \rangle_c$ channel are indicated in Fig. 3. There is one atom on each inner position for every four atoms in the rows defining the

---

[4]) In the following, directions and planes in the cubic cell are given an index "c", e.g. $[111]_c$, while notations in the hexagonal unit cell are given the index "h", e.g. $[001]_h$.
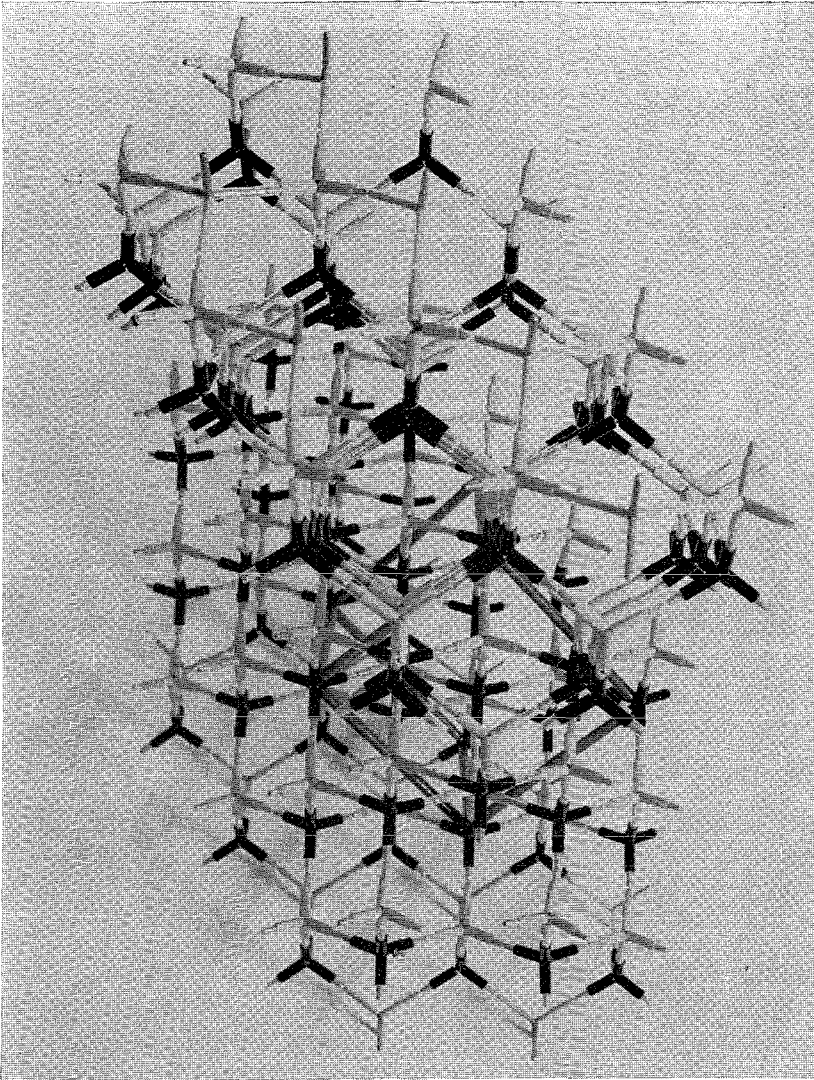
Fig. 2. Oblique view of the model of Fig. 1, looking down through a $\langle 110 \rangle_c$ channel of the upper sublayer. Four atoms of the lower sublayer, two of each kind, are located within the area of that channel, along its main diagonal. See also Fig. 3

channel. However, polytypism never introduces obstacles into those $\langle 110 \rangle_c$ channels whose directions are perpendicular to the c-axis. Fig. 1 shows this clearly.

5. Channeling Experiments in Si and SiC

5.1 Planar channels around $[111]_c$ in Si and $[001]_h$ in SiC

1 MeV He$^+$ ions are used throughout. To improve the counting statistics, a relatively large electronic window is applied on the backscattering spectrum, with discrimination levels at 515 and 389 keV. This corresponds to backscatter-

Fig. 3. The position of the atoms of one sublayer of SiC 6H with respect to an oblique $\langle 110 \rangle_c$ channel of an adjacent sublayer, given in units of 4.353 Å, the edge of the unit cube in a sublayer. See also Fig. 2
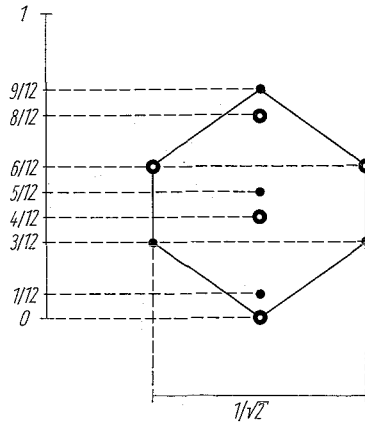
Table 1

Indices of certain directions and planes expressed in the hexagonal unit cell of SiC polytype 6H and in the cubic cell of one of the two sublayers

Directions		Planes	
cubic cell	hexagonal unit cell	cubic cell	hexagonal unit cell
[110]	[241]	(01$\bar{1}$)	($\bar{1}2\bar{1}0$)
[111]	[001]	($\bar{1}$01)	($\bar{1}1$20)
[112]	[$\bar{1}\bar{2}1$]	(1$\bar{1}$0)	(2$\bar{1}\bar{1}$0)
[113]	[8$\bar{1}\bar{6}5$]	(11$\bar{2}$)	(01$\bar{1}$0)
[114]	[$\bar{2}\bar{4}1$]	($\bar{2}$11)	($\bar{1}$010)
		(1$\bar{2}$1)	(1$\bar{1}$00)

ing from 0.1 to 0.28 μm below the surface in SiC. The window is thus 120 unit cells deep. In the case of Si, this same window corresponds to a penetration which is 14% deeper than in SiC. The Si wafers have surfaces cut closely perpendicular to the [111]$_c$ axis, and the SiC wafers have naturally grown surfaces perpendicular to the [001]$_h$ axis. The crystals are mounted on a target goniometer [1] whose axis of rotation φ is tilted by an angle $\alpha \approx 7°$ against the incident He$^+$ beam. The crystal is then rotated by a full turn ($\varphi = 0$ to 360°). The reproducibility of the setting is within a fraction of the critical angles in φ. Beam currents up to 25 nA were used, and no special efforts were undertaken to obtain the true widths and depths of the channels. Corrections for slight misalignments between the φ-axis of the goniometer and the [111]$_c$ or the [001]$_h$ axis have been applied (see Appendix C).

The experiment on Si was performed for comparison with SiC, and to test the reliability of our set-up. Although [111]$_c$ is only a threefold axis in Si, the backscattering yield itself has a sixfold symmetry (see Fig. 4). This is because the particular choice of $\alpha \approx 7°$ as a "random" angle does not uncover nonsymmetries in a given plane on both sides of [111]$_c$. The deep dips are due to the {110}$_c$ planes, while the shallower dips are caused by the less densely packed {112}$_c$ planes. The error in φ is at most 1°. According to equation (3), the min-
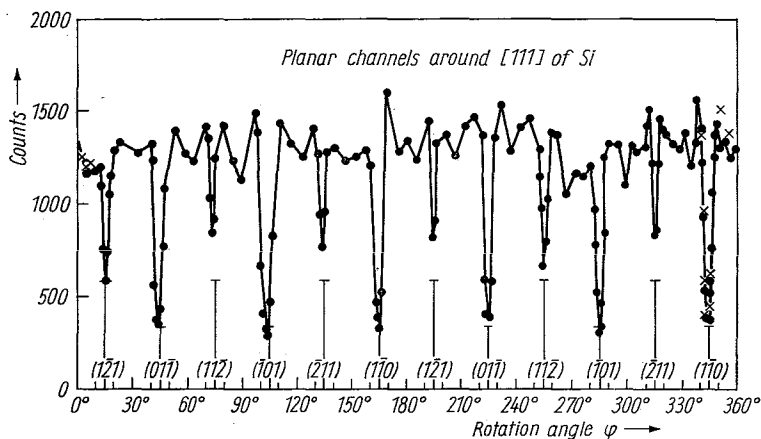
Fig. 4. Planar channeling obtained with 1 MeV He⁺ on a wafer of an Si single crystal. The $\langle 111 \rangle_c$ axis is tilted by $\alpha \approx 7.0°$ against the He⁺ beam, and the crystal is rotated by $\Delta\varphi = 386°$ around its $\langle 111 \rangle_c$ axis. Indices are given in the cubic unit cell of Si. The crosses indicate data obtained at angles φ exceeding 360° rotation
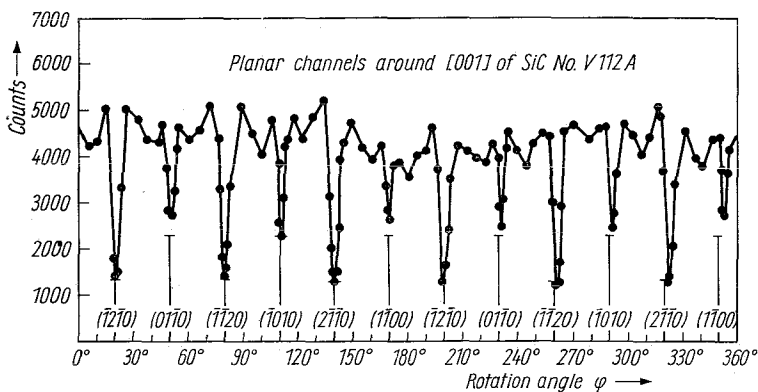
Fig. 5. Planar channeling obtained with 1 MeV He⁺ on the SiC crystal No. V112A for $\alpha \approx 7.0°$ and $\Delta\varphi = 385°$. Note the similarity with Fig. 4. Indices are given in the hexagonal unit cell of SiC 6 H

ima should have a ratio of $\sqrt{3}$. These levels are indicated in Fig. 4, after normalization to the average $\{110\}_c$ minimum yield. The apparent discrepancy may stem from the relatively wide window and from the fact that no depth correction [8] was applied.

The results of the same experiment performed on an SiC crystal are shown in Fig. 5. The positions and relative intensities of the minima predicted by the 6H model are identical to those of Si, assuming that the presence of C atoms in the planes does not invalidate equation (3). The theoretical minima are again plotted in the figure after normalization to the average yield of the $\{2\bar{1}\bar{1}0\}_h$ minima. As a whole, Fig. 4 and 5 are closely similar. Polytypism of SiC does therefore not lead to significant differences with respect to Si in a planar channeling experiment around $[001]_h$.

5.2 Axial channels in the {110}$_c$ planes of Si and the {211}$_h$ planes of SiC

That the symmetry of the [111]$_c$ axis of Si is threefold, and not sixfold, can be demonstrated by backscattering if the tilt angle α with respect to [111]$_c$ is varied on either side of this axis while the beam remains aligned in a plane. We selected a {110}$_c$ plane in Fig. 4 and measured the yield in this plane, varying α up to 40° on either side of [111]$_c$ (Fig. 6). In this experiment, the rotation angle φ was an adjustable parameter to insure the alignment of the beam with the plane. The dips now correspond to specific axes. Their position and relative depths are calculated and plotted into Fig. 6 as well (see Appendix B and equation (1)). The depths of the nine measured dips follow exactly the predicted ranking. The two sides of the plot are clearly dissimilar, as expected from the threefold symmetry of the [111]$_c$ axis of Si. Note in particular that the two axes [110]$_c$ and [114]$_c$ have symmetrical positions (calculated as 35.27° off [111]$_c$) but quite different depths. Also note that the positions located symmetrically to the prominent [112]$_c$ and [113]$_c$ dips do not show a significant deviation from the "random" level.[5] As a whole, Fig. 6 conforms properly to expectations.
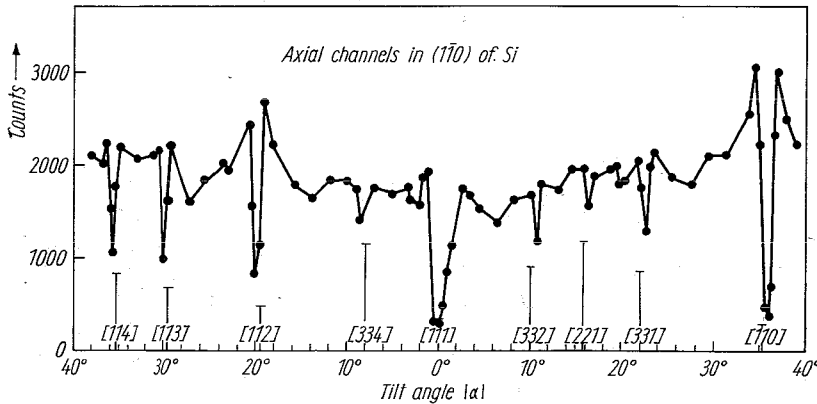
Fig. 6. The minimum yield in a {1$\bar{1}$0}$_c$ planar channel of Si (see Fig. 4) for variable tilt angle α ($\varphi \approx$ const) on either side of the $\langle 111 \rangle_c$ axis. The theoretical positions of the channels are given on the abscissa. The bars there are expected minimum yields on a relative scale. Indices are given in the cubic cell of Si
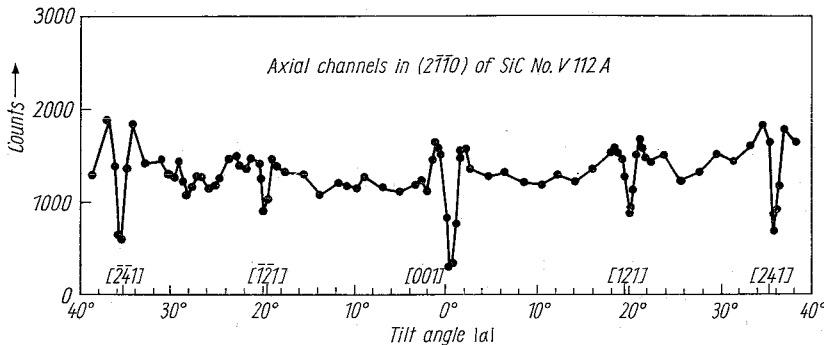
Fig. 7. The minimum yield in a {2$\bar{1}\bar{1}$0}$_h$ planar channel of the SiC crystal No. V112A (see Fig. 5) for variable tilt angle α ($\varphi \approx$ const) on either side of the $\langle 001 \rangle_h$ axis. The theoretical positions of the channels are given on the abscissa. Indices are given in the hexagonal unit cell of SiC 6H

[5] Table 3 indicates that the [552]$_c$ axis at the mirror position of [112]$_c$ ranks No. 12 in the intensity scale. The mirror position of [113]$_c$ is [771]$_c$ which ranks No. 20. In general, mirror axes will have indices [hhl]$_c$ and [h'h'l']$_c$ with $h' = 1 + 2\, l/h$, $l' = 4 - l/h$.

The result of a similar experiment performed on a SiC crystal is given in Fig. 7. The data differ radically from those of Fig. 6. First, the pattern is now symmetrical with respect to $[001]_h$. Second, identifiable dips are few and shallow. Five dips can be identified which correspond to $[114]_c$, $[112]_c$, $[111]_c$, an axis located symmetrically to $[112]_c$, and $[110]_c$. A special search to look for the equivalent of $[113]_c$ did not produce any dip.

Note that the "random" level in Fig. 6 and 7 actually corresponds to the minimum of a planar $\{110\}_c$ or $\{2110\}_h$ channel.

6. Discussion

Fig. 7 is compatible with the sixfold symmetry of the $[001]_h$ axis for SiC 6H. We did not measure the axial channels in the two remaining $\{2110\}_h$ planes, but Fig. 5 and 7 together leave no alternative but that of sixfold symmetry. In Si, the $[110]_c$ channel is most pronounced (Fig. 6) while in SiC, $[001]_h$ dominates. This can be explained by the fact that the diamond lattice exhibits large voids in the $\langle 110 \rangle_c$ directions (corresponding to a small value of d_a), while in SiC the voids in the $\langle 241 \rangle_h$ directions are rather more intricate (see Fig. 2 and 3). To our knowledge, no model has yet been developed for channeling and backscattering through channels of this structural complexity. The simple Lindhard model [8] of axial channeling along a string of atoms is one-dimensional and does not include the case of channels formed by differently populated strings. $\langle 241 \rangle_h$ channels of SiC 6H represent such a case, but with two additional complications: (i) Each row composing the contour of the channel is interrupted in every other sublayer, thus forming clusters of four atoms, each followed by a void of equal length along the row. (ii) In those interrupted segments, four atoms are located within the channel area. There appear two ways of calculating the effects on channeling of such atoms "within a channel": (i) These atoms form additional rows to be treated as the others according to Lindhard. (ii) They constitute obstacles within the channel and thus weaken the channeling process. The former treatment gives a ratio of the minimum yields of the $\langle 001 \rangle_h$, $\langle 241 \rangle_h$, and $\langle 121 \rangle_h$ dips of $1:(3/2)\sqrt{3/2}:3\sqrt{2} = 1:1.8:4.2$, while the experiments give $1:1.7:2.8$.

Evidently, the gross features of Fig. 7 are explainable from the properties of polytype 6H. The full interpretation demands more detailed experimentation as well as a better theory for such complex channels.

7. An SiC Crystal with Intermediate Properties

Fig. 8 was obtained on a different SiC crystal (SiC 6, see Table 2), with the same measurements as in Fig. 6 and 7. Fig. 8 shows features intermediate between those of Fig. 6 and 7.[6]) Apart from the most pronounced $[111]_c$ channel we find channels of nonequal intensities in the $[1\bar{1}0]_c$ and $[114]_c$ directions, respectively. The same is true for the $[112]_c$ channel and its symmetrical direction. A careful search around 30° on either side of the $[111]_c$ dip even revealed two $[113]_c$ dips, although the one on the right side of the figure is barely identifiable. We thus find dips at 20° and 30° to the right (indicated by the dashed lines on the abscissa) where none are found in Si. These "mirror" dips are weaker than their original counterparts (e.g. $[112]_c$ and "$[112]_c$"), but they intensify a dip if they coincide with another original dip, as is the case with $[114]_c$ and

---

[6]) In the following discussion we use the cubic notation for SiC sample No. 6.
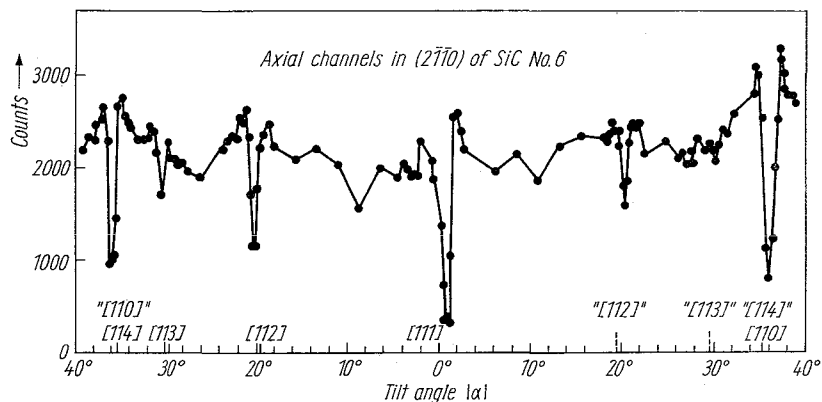
Fig. 8. The minimum yield in a $\{2\bar{1}\bar{1}0\}_h$ planar channel of the SiC crystal No. 6 for variable tilt angle α ($\varphi \approx$ const) on either side of the $\langle 001 \rangle_h$ axis. The theoretical positions of the channels are given on the abscissa with indices in the cubic unit cell of Si (compare with Fig. 6). The channels occurring at mirror image points are identified by dashed lines and labelled in quotation marks. They are absent in Si

"$[114]_c$". The mirror dip "$[113]_c$" is not so clearly identified, but the $[113]_c$ dip is also the weakest of the original channels found in the figure. A closer analysis of records such as Fig. 8 in terms of polytype content at a certain depth of a crystal appears feasable.

8. Comparison with X-Ray Studies

Laue transmission patterns were obtained from the two SiC crystals No. V 112 A and No. 6 studied. The results, together with other data, are given in Table 2. They show that the crystal No. V112A as a whole consists of polytypes 6H and 21R. On the other hand, the crystal No. 6 is composed of several polytypes. It should be noted, however, that the mean range of the Cu X-rays used in the transmission is about 70 μm, whereas the backscattering information stems from the depth of 0.1 to 0.28 μm below the surface. Detailed comparison

Table 2

Data on SiC specimens No. V112A and No. 6

SiC sample	No. V 112 A	No. 6
Growth temperature (°C)	2500	?
Doping (cm⁻³)	n-type (5×10^{18} to 10^{19})	p-type (?)
Thickness (mm)	1.1	0.21
Approx. area (mm²)	20	10
Appearance	transparent (light green)	opaque (black)
Qualitative composition from transmission Laue pattern	21R and 6H	15R, 6H, and some 4H possibly some 15R in screwed position

of backscattering patterns after repeated etching of surface layers can thus produce specific information about the structural composition of such crystals, and the integral composition can then be compared to the X-ray patterns.

The two techniques of backscattering and X-ray studies complement rather than replace each other. For instance, X-ray and backscattering data together strongly suggest that our SiC specimens are layered combinations of polytypes. The crystals are small platelets whose surface is perpendicular to the c-axis. Their surface area much exceeds the cross-section of the X-ray or the He$^+$ beam. Yet, both the Laue and the backscattering patterns hardly change throughout the area of the samples. A difference in the result between the two must then mean that the crystals are layered.

9. [001]$_h$ Channel of SiC Sample V112B

To test the quality of our SiC crystals we measured the [001]$_h$ channel of sample No. V112B, which was grown in the same batch as No. V112A and is of similar appearance. In this experiment some efforts were undertaken to keep the beam divergence small, and to avoid surface contamination and radiation damage of the crystal.[7] A beam current of 3 to 5 nA was used. Fig. 9 shows that the channel is well shaped with a critical angle $\psi_{1/1} = 1.5°$. Equation (2) gives $\psi_{1/1\,a} = 1.4°$, with $d_a = 15.1$ Å and $\overline{Z_2} = 40$ (two Si and two C atoms per unit cell along the c-axis). In this case the window was placed to equivalent depths of 0.12 and 0.34 μm. No corrections for surface transmission, depth dependence, and thermal vibrations are applied. The above result agrees reasonably well with a previously measured value [7] of $\psi_{1/1} = 2.25°$ at a He$^+$ energy of 0.5 MeV.[8] The minimum yield χ is measured as 0.08. Equation (1) gives $\chi = 0.04$ with $a = 0.19$ Å (mean Thomas-Fermi radius of C and Si), $N = 9.7 \times 10^{22}$ atoms/cm^3, $d_a = (1/4) \times \times 15.1$ Å. Here, we assumed that all
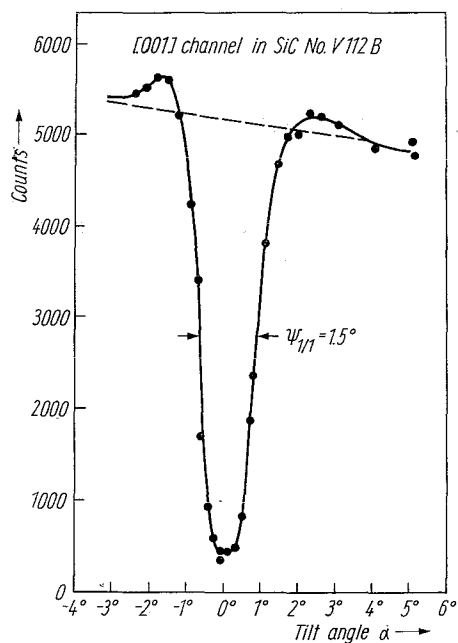
Fig. 9. Channeling in the $\langle 001 \rangle_h$ direction of SiC measured on sample No. V112B, observed by backscattering of 1 MeV He$^+$ ions. Measured values: $\psi_{1/1} = 1.5°$ and $\chi_{min} = 8\%$; the theoretical values are 1.4° and 4%. Indices are given in the hexagonal unit cell of SiC 6H

---

[7] After about 40 μAs of integrated beam current we observed a significant increase of the minimum yield due to surface contamination, so the spot of impact was changed in shorter intervals. In addition, we observed a darkening of the crystal, which did not disappear when a surface layer was removed by oxidation at 1200 °C and etching in HF, and is thus attributed to radiation damage inside the crystal.

[8] The discrepancy with the calculated value of $\psi_{1/1}$ in reference [7] is due to the erroneous assumption of 6 Si and 6 C atoms in the unit cell along the c-axis (private communication with the authors).

atomic rows contribute equally to the minimum yield. We feel that the measured valueof 0.08 constitutes but an upper limit because no corrections are applied, so that no discrepancy with the calculated value can be claimed.

10. Conclusion

Backscattering offers a new possibility to study polytypism in the first few microns of a crystal, and with differential depth resolution. The present results demonstrate the feasibility of this method. But this study also leaves many and new questions unanswered. For instance, one should expect that in directions perpendicular to the c-axis, channeling and backscattering are not affected by polytypism. We attempted but failed to show this conclusively because our specimens were not thick enough. More generally: To what extent can backscattering differentiate polytypes ? Can simple models be developed to describe channeling and backscattering in diatomic structures of the complexity exhibited in the polytypes of SiC ? For applications it is most important to be able to identify accurately the polytype of single crystals in its outer layers. Devices depend usually critically on the physical properties at interfaces, and it is known that the energy gap of SiC increases from 2.2 eV to well above 3 eV as the polytype changes [5].

At the time of this writing an article by Barrett [6] just appeared in which yet unpublished work on SiC is discussed. The author reports on polytype identification from photographs of blocking patterns and from the relative intensities of the recorded lines. A comparison with computed tables of line intensities then reveals the polytype in the surface layer of the crystal. This technique is closely similar to that of backscattering, and appears to be successful with less experimental effort if structure identification is the sole aim. Backscattering, on the other hand, possesses differential depth resolution and is applicable also to the detection of lattice impurities [4] and their crystallographic position, properties which simple photographic records all lack.

Appendix A

Mean range of 1 MeV He$^+$ in SiC

From Siffert and Coche ([3], p. 282), the range of α-particles of 1 MeV in Si is taken as $R_{Si} = 1.02$ g/cm^3. The same curve was used to estimate the range in C, R_C, by recalibration of the scales in dimensionless energy and range units (same reference, p. 284). Finally the range in SiC, R_{SiC}, was estimated through $R_{SiC} = (1/R_{Si} + 1/R_C)^{-1}$, which results in $R_{SiC} = 3.8$ μm (compared to $R_{Si} = 4.4$ μm in Si). The densities used are $\varrho_{Si} = 2.33$ g/cm^3, and $\varrho_{SiC} = 3.22$ g/cm^3.

dE/dx for 1 MeV He⁺ in SiC

a) From reference [3], dE/dx of Si in Si has a maximum of 31 eV/Å. A value of 30 ± 1.5 eV/Å is correct between $E_{min} = 0.28$ MeV and $E_{max} = 1.1$ MeV. For Si in SiC we have then 29.1 eV/Å.

b) dE/dx in C is estimated by two methods:

(i) From Whaling ([3], p. 203), we extrapolated a value of 5.8 eV/Å for dE/dx of C in SiC.

(ii) The estimate $(dE/dx$ in C) = $(dE/dx$ in Si) $\cdot (R_{Si}/R_C)$ gives 5.5 eV/Å, if the atomic density of C were equal to that of Si in Si. Correcting for this difference we find $(dE/dx$ of C in SiC) = 5.3 eV/Å.

c) $(dE/dx$ in SiC) = 29.1 eV/Å + 5.5 eV/Å $\approx$ 35 eV/Å.

Depth resolution for backsattering in SiC

The energy loss per unit cell along the c-direction forth and back is 70 eV/Å $\times$ $\times$ 15.1 Å/unit cell = 1.1 keV/unit cell. If the energy analysis is done by Si-charged particle detectors, Siffert and Coche ([3], p. 286) give a limit of energy resolution of 5 keV for α-particles of 1 MeV due to nuclear collisions. If this resolution is achieved, a depth resolution of (5 keV/1.1 keV) unit cell = = 4.5 unit cells follows. In the present experiments, the energy resolution lies between 10 and 15 keV.

Appendix B

Axial channels in the $(1\bar{1}0)_c$ plane of the diamond lattice

The angles between the axial channels and the $[110]_c$ axis can be calculated by

$$\tan \varphi_{AA} = \tan \varphi_{BB} = \frac{2\,n}{m}\frac{\sqrt{2}}{2} \quad \text{and} \quad \tan \varphi_{AB} = \frac{4\,n \pm 1}{2\,m \mp 1}\frac{\sqrt{2}}{2}. \quad (A1)$$

Table 3

The 15 most prominent dips in the $(1\bar{1}0)_c$ plane
of a diamond lattice, between the $[114]_c$ axis
and the $[110]_c$ axis

Axis	Angle	d_a/g	Rank
[110]	35.27°	0.707	1
[551]	27.22°	3.570	11
[331]	22.00°	2.179	6
[552]	19.47°	3.674	12
[221]	15.78°	3.000	9
[553]	12.28°	3.841	13
[332]	10.03°	2.345	7
[554]	5.77°	4.062	14
[111]	0°	0.866	2
[334]	− 8.05°	2.915	8
[335]	−14.42°	3.279	10
[112]	−19.47°	1.225	3
[337]	−23.52°	4.093	15
[113]	−29.50°	1.658	4
[114]	−35.27°	2.121	5

The axes are then $[m, m, 2n]_c$ and $[2m \pm 1, 2m \pm 1, 4n \pm 1]_c$ $(n, m = 0, \pm 1, \pm 2, \ldots)$. (In SiC, A and B denote the two kinds of atoms.)

The $[111]_c$ axis is given by $\tan \varphi_{AB} = \sqrt{2}/2$, $\varphi_{AB} = 35.27°$.

The average separation of atoms along an axis is given by

$$\frac{d_a}{g_{AA}} = \frac{\sqrt{2}}{2} \frac{m}{\cos \varphi_{AA}} \quad \text{and} \quad \frac{d_a}{g_{AB}} = \frac{\sqrt{2}}{2} \frac{2m+1}{\cos \varphi_{AB}} \; ; \quad g = \text{lattice constant} . \quad \text{(A2)}$$

According to equation (1), the minima of the dips are proportional to d_a. We thus define the rank of the dips according to the magnitude of $1/d_a$. In Table 3, the 15 most prominent dips in the $(1\bar{1}0)_c$ plane are given, together with their angular positions relative to the $[111]_c$ axis, the normalized spacing d_a/g, and the rank.

Appendix C

Correction for misalignment of the c-axis and the axis of rotation of the goniometer

In commercial Si wafers, which are cut perpendicular to the $[111]_c$ axis, as well as in the SiC samples we used, the misalignment never exceeded a few degrees. The required corrections are therefore of minor nature, when the crystal axis rather than the φ-axis is used as reference axis for directional indications.

If the crystal axis is lined up with the He$^+$ beam at a tilt angle α_1 and an azimuthal angle φ_1, and a given other direction $\boldsymbol{P_0}$ at angles α_0 and φ_0, then the angles of $\boldsymbol{P_0}$ with respect to the crystal axis, α and φ, are calculated through the laws of spherical trigonometry as

$$\varphi = \varphi_1 + \sin^{-1}\left[\sin (\varphi_0 - \varphi_1) \frac{\sin \alpha_0}{\sin \alpha}\right] ; \quad \text{(A3)}$$

$$\alpha = \cos^{-1}\left[\cos \alpha_0 \cos \alpha_1 + \sin \alpha_0 \sin \alpha_1 \cos (\varphi_0 - \varphi_1)\right] .$$

The raw data were corrected in this manner to obtain Fig. 6, 7, and 8.

Fig. 4 and 5 require a slightly different kind of adjustment. Since the position of the crystal axis was not measured, the 12 dips were plotted on a stereogram [1, 4], and corresponding dips (at about 180°) connected by straight lines.[9]) A circle was then drawn around the common intersection, and the angles φ were then measured on that circle.

References

[1] J. U. ANDERSON, J. A. DAVIES, K. O. NIELSEN, and S. L. ANDERSON, Nuclear Instrum. and Methods **38**, 210 (1965). See also other papers in that issue.

[2] C. D. HODGMAN (Ed.), Handbook of Chemical Physics, 44th edition, Chemical Rubber Publ. Co., Cleveland, Ohio 1963 (p. 2767).

[3] W. WHALING, in: Hdb. Phys., Vol. 34, Ed. S. FLÜGGE, Springer-Verlag, Berlin 1958. P. SIFFERT and A. COCHE, in: Semiconductor Detectors, Ed. G. BERTOLINI and A. COCHE, North-Holland Publ. Co., Amsterdam 1968 (pp. 279 to 300). See also Appendix A of this paper.

---

[9]) Actually, the lines connecting two dips in a stereogram follow an equation

$$\alpha = \sin^{-1}\{\cos \alpha_1 [1 - \sin^2 \alpha_1 \sin^2 (\varphi - \varphi_1)]^{-1/2}\} ,$$

where the angles are defined above. For $\alpha \leqq 10°$, the difference to the straight-line approximation $\alpha = \cos \alpha_1/\cos (\varphi - \varphi_1)$ (in polar coordinates) never exceeds 1%.

[4] J. W. Mayer and O. J. Marsh, Ion Implantation in Semicondutors, in: Applied Solid State Science, 1, Academic Press, New York 1969.

[5] A. R. Verma and P. Krishna, Polymorphism and Polytypism in Crystals, J. Wiley & Sons, New York 1966; see also: SiC Data Table and Suppl. Bibliography, EPIC Interim Rep. No. 62, Hughes Aircraft Co., Electronic Properties Information Center, Culver City (Calif.) 1968.

[6] C. S. Barrett, Naturwissenschaften 57, 287 (1970).

[7] Hj. Matzke and M. Königer, phys. stat. sol. (a) 1, 469 (1970).

[8] J. Lindhard, Mat.-Fys. Medd. Dan. Vid. Selsk. 34, No. 14 (1965). Experimental tests see, e.g., S. T. Picraux, Thesis, Calif. Inst. Technology, Padasena (Calif.) 1969.

(Received September 7, 1970)

Note added in proof:

At the "International Conference on Radiation Effects in Semiconductors", Albany, New York 1970, Hart, Dunlap, and Marsh have presented results on measurements of ψ_a along the same $[001]_h$-axis at 280 keV (to be published in Radiation Effects). The results now available are as follows:

	$\psi_{1/1a}$ along $[001]_h$	E_α(keV)	SiC polytype
Hart et al.	$1.35° \pm 0.1°$	280	15R
Matzke and Königer [7]	$1.15°$	500	6H (?)
present work	$0.75°$	1000	6H and 21R

A least squares fit yields
$$\psi_{1/1,\,[001]_h} = 19.47 \times E \text{ (keV)}^{-0.467} \sim E^{-0.5}.$$